IOPscience iopscience.iop.org

Home Search Collections Journals About Contact us My IOPscience

Rényi entanglement entropies in quantum dimer models: from criticality to topological order

This article has been downloaded from IOPscience. Please scroll down to see the full text article.

J. Stat. Mech. (2012) P02003

(http://iopscience.iop.org/1742-5468/2012/02/P02003)

View the table of contents for this issue, or go to the journal homepage for more

Download details:
IP Address: 132.166.62.115
The article was downloaded on 18/10/2012 at 11:55

Please note that terms and conditions apply.

Journal of Statistical Mechanics: Theory and Experiment
An IOP and SISSA journal

Rényi entanglement entropies in quantum dimer models: from criticality to topological order

Jean-Marie Stéphan, Grégoire Misguich and Vincent Pasquier

Institut de Physique Théorique, CEA, IPhT, CNRS, URA 2306, F-91191 Gif-sur-Yvette, France
E-mail: jean-marie.stephan@cea.fr, gregoire.misguich@cea.fr and vincent.pasquier@cea.fr

Received 26 October 2011
Accepted 28 December 2011
Published 3 February 2012

Online at stacks.iop.org/JSTAT/2012/P02003
doi:10.1088/1742-5468/2012/02/P02003

Abstract. Thanks to Pfaffian techniques, we study the Rényi entanglement entropies and the entanglement spectrum of large subsystems for two-dimensional Rokhsar–Kivelson wavefunctions constructed from a dimer model on the triangular lattice. By including a fugacity t on some suitable bonds, one interpolates between the triangular lattice ($t = 1$) and the square lattice ($t = 0$). The wavefunction is known to be a massive $\mathbb{Z}_2$ topological liquid for $t > 0$ whereas it is a gapless critical state at $t = 0$. We mainly consider two geometries for the subsystem: that of a semi-infinite cylinder and the disc-like set-up proposed by Kitaev and Preskill (2006 *Phys. Rev. Lett.* **96** 110404). In the cylinder case, the entropies contain an extensive term—proportional to the length of the boundary—and a universal subleading constant $s_n(t)$. Fitting these cylinder data (up to a perimeter of $L = 32$ sites) provides s_n with a very high numerical accuracy (10^{-9} at $t = 1$ and 10^{-6} at $t = 0.5$). In the topological $\mathbb{Z}_2$ liquid phase we find $s_n(t > 0) = -\ln 2$, independent of the fugacity t and the Rényi parameter n. At $t = 0$ we recover a previously known result, $s_n(t = 0) = -\frac{1}{2}\ln(n)/(n-1)$ for $n < 1$ and $s_n(t = 0) = -\ln(2)/(n-1)$ for $n > 1$. In the disc-like geometry—designed to get rid of the boundary contributions—we find an entropy $s_n^{\mathrm{KP}}(t0) = -\ln 2$ in the whole massive phase whatever $n > 0$, in agreement with the result of Flammia *et al* (2009 *Phys. Rev. Lett.* **103** 261601). Some results for the gapless limit $R_n^{\mathrm{KP}}(t \to 0)$ are discussed.

©2012 IOP Publishing Ltd and SISSA
1742-5468/12/P02003+30$33.00

Keywords: conformal field theory (theory), dimers (theory), entanglement in extended quantum systems (theory)

ArXiv ePrint: 1108.1699

Contents

1. Introduction **3**

2. Entanglement entropy as a Shannon entropy **4**
2.1. Rokhsar–Kivelson wavefunctions 4
2.2. Rényi entanglement entropy 5
2.3. Schmidt decomposition 5

3. Classical probabilities **7**
3.1. Pfaffian 7
3.2. Kasteleyn theory 7
3.3. Classical probabilities 8
3.4. Perturbation theory for determinants in an infinite system 8

4. Results for the infinite cylinder **10**
4.1. Topological entanglement entropy and Rényi index 10
4.2. Thermodynamical entropy 11
4.3. Scaling when $t \to 0$ and $L \to \infty$ with fixed $L \cdot t$ 13
4.4. Entropy of a zig-zag line 14
4.5. Infinite Rényi and bipartite fidelity 15
4.6. Entanglement gap and entanglement spectrum 16

5. Long strip geometry **19**

6. Kitaev–Preskill construction **20**

7. Summary and conclusions **23**

Appendix A. Green function elements for an infinite cylinder **24**
A.1. Diagonalization of the Kasteleyn matrix 24
A.2. Green function elements 25

Appendix B. Closed-form formula for $S_{n=\infty}$ in the cylinder geometry **26**
B.1. Dimer coverings on a finite cylinder 26
B.2. Exact formula for $S_{n=\infty}$ 28
B.3. Asymptotic expansion 29

References **29**

J. Stat. Mech. (2012) P02003

1. Introduction

It is now widely recognized that the entanglement entropy is a useful quantity to probe many-body quantum states. It can be used to detect critical states in one-dimensional chains, through the celebrated logarithmic divergence [1]–[4]. In two dimensions it can be used to characterize (massive) topologically ordered states. In particular, it allows us to distinguish a topological wavefunction from a more conventional disordered and featureless state. In a gapped phase the entanglement entropy of a large subsystem contains a contribution proportional to the length (in two dimensions) of its boundary plus a subleading term $S_{\rm topo}$ which contains some information about the nature of the phase. In a state with topological order, this subleading term is related to the total quantum dimension, that is, to the content in elementary excitation [5]–[7]. This idea has been successfully applied to some fractional quantum Hall states [8]–[10]. Extracting the subleading term in lattice models is not a trivial task [6, 7] but it was first shown to be feasible using quantum dimer wavefunctions on the triangular lattice [11]. Since the work of Moessner and Sondhi [12] these types of states have been intensively studied since they offer some rather simple realization of topologically ordered states with non-trivial finite-size effects and finite correlation length (contrary to toric-code-like models [13, 14]).

In this paper we also consider some dimer wavefunctions—named after Rokhsar and Kivelson (RK) [15]—which are linear superpositions of fully packed dimer coverings on the triangular lattice. By including a fugacity on some suitable bonds, one continuously interpolates between the triangular lattice ($t = 1$) and the square lattice ($t = 0$). In the triangular case the wavefunction is known to be a massive $\mathbb{Z}_2$ topological liquid [12, 16, 17], whereas it is a gapless critical state at $t = 0$ [15]. Exploiting previous results [11, 18] on the reduced density matrix (RDM) of RK states, we can obtain not only the entanglement entropy but also the full entanglement spectrum on large systems. Using extensively the Pfaffian formulation of the classical dimer partition function [19], as well as some perturbation theory for determinants [20, 16], we perform calculations *in the thermodynamic limit* while keeping the boundary length finite.

In the cylinder geometry we can treat the infinite-height limit and perimeters up to $L = 32$ (38 at $t = 0$). In the disc-like geometry proposed by Kitaev and Preskill [6], we perform exact calculations for discs of radii up to $\rho \simeq 4.5$ lattice spacings embedded in an *infinite* system, therefore extending significantly the previous entanglement calculations on triangular dimer wavefunctions [11]. This technique allows us to confirm the value $S_{\rm topo} = -\ln(2)$ with high precision in the whole massive phase (not only at the triangular point $t = 1$). This value turns out not to depend on the Rényi parameter, in agreement with the argument by Flammia *et al* [21]. We also discuss the structure of the *entanglement spectrum*, showing that it contains a non-degenerate 'ground state' and a gap. In section 4.6, a microcanonical point of view is used to relate the density of states of the entanglement spectrum and the Rényi entanglement entropies.

When $t = 0$ the dimers are restricted to the bonds of a square lattice. Although non-generic[1], such critical RK wavefunctions associated with some conformally invariant critical points are useful since they offer one of the very few situations where one can study the entanglement in a critical wavefunction in more than one dimension [25, 26, 18, 27, 28].

[1] They correspond to fine-tuned multi-critical points [22]–[24].

J. Stat. Mech. (2012) P02003

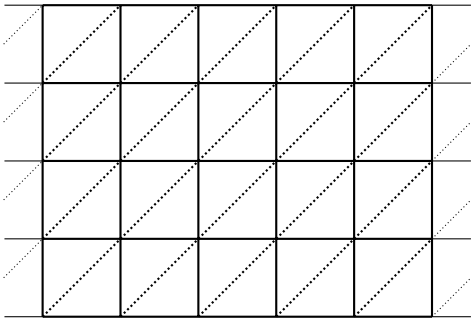

Figure 1. Triangular lattice with cylindrical boundary conditions ($L_x = 6$, $L_y = 5$). Each 'diagonal link' (dotted lines) has fugacity t, while the others have fugacity 1.

Another point of view is that, for long cylinder geometries, the entanglement in these two-dimensional systems is related to the Shannon entropies in—now generic—quantum critical chains [18], [29]–[31]. The subleading constant in the cylinder geometry depends on the compactification radius [26, 18, 27, 28] and shows a singularity at some critical value of the Rényi parameter [31]. The result in a Kitaev–Preskill geometry is less clear and we discuss our numerical results at the end of section 6.

2. Entanglement entropy as a Shannon entropy

After a brief introduction to dimer RK wavefunctions [15], we review how one can construct the RDM and Schmidt decomposition for these states.

2.1. Rokhsar–Kivelson wavefunctions

We start from a classical two-dimensional hard-core dimer model on a triangular lattice, with fugacity t on 'diagonal' links (figure 1). This fugacity allows us to interpolate between the square lattice ($t = 0$) and the isotropic triangular lattice ($t = 1$).

The classical partition function of this system is

$$\mathcal{Z} = \sum_{\mathrm{c}} \mathrm{e}^{-E(c)} = \sum_{\mathrm{c}} t^{\#\ \text{diagonal dimers}}, \tag{1}$$

where the sum runs over all dimer coverings c. When $t = 0$ (square lattice), the model is known to be critical [20, 32] and its long range behavior is described by a compact free field [33, 34]. Otherwise it has a finite correlation length [12, 16, 17]. An Hilbert space is then constructed by associating a basis state $|c\rangle$ to each classical dimer configuration c. Different classical configurations correspond to orthogonal states. The RK wavefunction is the normalized linear combination of all basis states with an amplitude equal to the square root of the classical weight:

$$|\mathrm{RK}\rangle = \frac{1}{\sqrt{\mathcal{Z}}} \sum_{\mathrm{c}} \mathrm{e}^{-E(c)/2} |c\rangle. \tag{2}$$

J. Stat. Mech. (2012) P02003

Following Henley [35] one can construct some local Hamiltonians for which equation (2) is an exact ground state, but the precise form of these Hamiltonians will not be used in the following.

2.2. Rényi entanglement entropy

We divide the system into two parts A and B. Each subsystem is a set of bonds, and its degrees of freedom are the corresponding dimer occupancies. The RDM of A is obtained by tracing over the degrees of freedom in B:

$$\rho_A = \mathrm{Tr}_B\, |RK\rangle\langle RK|. \tag{3}$$

Then, the Rényi entanglement entropy is defined as

$$S_n = \frac{1}{1-n} \ln \mathrm{Tr}\, \rho_A^n, \tag{4}$$

where n is not necessarily an integer. Two limits are of interest. For $n \to 1$, S_n reduces to the von Neumann entanglement entropy:

$$S_1 = S^{\mathrm{vN}} = -\,\mathrm{Tr}\, \rho_A \ln \rho_A. \tag{5}$$

For $n \to \infty$, only the largest eigenvalue $p_{\max}$ of the RDM matters:

$$S_\infty = -\ln p_{\max}. \tag{6}$$

This quantity is also called single-copy entanglement. To compute all the Rényi entropies, we need all the eigenvalues of the RDM. In the following, we shall see that calculating each eigenvalue amounts to solving a combinatorial problem. The procedure has been discussed in detail elsewhere [11, 18] and is recalled below for completeness.

2.3. Schmidt decomposition

We consider the geometry of an infinite cylinder cut into two parts, as in the left of figure 2. The reasoning is the same for the other geometries we considered. The sites which touch a bond in A and an bond in B (red circles in figure 2) are called boundary sites. We assign a spin σ_j to each boundary site: $\sigma_j = \uparrow$ if the site is occupied by a dimer in A and $\sigma_j = \downarrow$ if it is occupied by a dimer in B. We denote by

$$|i\rangle = |\sigma_1, \sigma_2, \ldots, \sigma_{L_x}\rangle \tag{7}$$

the whole spin configuration at the boundary.

Now, let $\mathcal{E}_i^A$ (resp. $\mathcal{E}_i^B$) be the set of dimer configurations in A (resp. B) compatible with $|i\rangle$ at the boundary. Thanks to the hard-core constraint, they share no common element:

$$\mathcal{E}_i^A \cap \mathcal{E}_{i'}^B = \emptyset, \qquad i \neq i'. \tag{8}$$

Each configuration c can be written as

$$c = a \cup b, \qquad a \in \mathcal{E}_i^A, \qquad b \in \mathcal{E}_i^B \tag{9}$$

and the energy decomposed as

$$E(c) = E_A(a) + E_B(b). \tag{10}$$

J. Stat. Mech. (2012) P02003

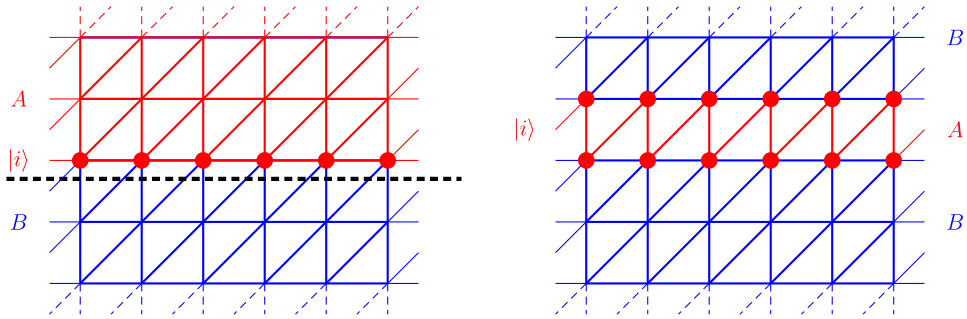

Figure 2. Partition of the lattice in two subsystems A (red bonds) and B (blue bonds). Left: the subsystems A and B are semi-infinite cylinders. Boundary sites are marked by filled red circles. Each boundary site can either be occupied by a dimer in A (spin $\uparrow$) or a dimer in B (spin $\downarrow$).

This allows us to write the RK state as

$$|RK\rangle = \frac{1}{\sqrt{\mathcal{Z}}} \sum_i \left[\sum_{a \in \mathcal{E}_i^A} \mathrm{e}^{-E_A(a)/2} |a\rangle \right] \times \left[\sum_{b \in \mathcal{E}_i^B} \mathrm{e}^{-E_B(b)/2} |b\rangle \right]. \tag{11}$$

Defining a new normalized set of RK states in A and B

$$|\mathrm{RK}_i^A\rangle = \frac{1}{\sqrt{\mathcal{Z}_i^A}} \sum_{a \in \mathcal{E}_i^A} \mathrm{e}^{-\frac{1}{2}E_A(a)} |a\rangle, \tag{12}$$

$$|\mathrm{RK}_i^B\rangle = \frac{1}{\sqrt{\mathcal{Z}_i^B}} \sum_{b \in \mathcal{E}_i^B} \mathrm{e}^{-\frac{1}{2}E_B(b)} |b\rangle, \tag{13}$$

$$\text{with } \mathcal{Z}_i^\Omega = \sum_{\omega \in \mathcal{E}_i^\Omega} \mathrm{e}^{-E_\Omega(\omega)} \qquad (\Omega = A, B), \tag{14}$$

equation (2) becomes

$$|RK\rangle = \sum_i \sqrt{p_i} |RK_i^A\rangle |RK_i^B\rangle, \tag{15}$$

with

$$p_i = \frac{\mathcal{Z}_i^A \mathcal{Z}_i^B}{\mathcal{Z}}. \tag{16}$$

Equation (15) is actually the Schmidt decomposition of the RK state (the orthogonality of the Schmidt vectors is guaranteed by equation (8)), and the $\{p_i\}$ are the eigenvalues of the RDM:

$$\rho_A = \sum_i p_i |RK_i^A\rangle\langle RK_i^A|. \tag{17}$$

J. Stat. Mech. (2012) P02003

This way, one can obtain the Rényi entropy:

$$S_n = \frac{1}{1-n} \ln \left(\sum_i p_i^n \right). \tag{18}$$

The entanglement entropy calculation has been reduced to finding some probabilities in the classical dimer problem. In section 3 we will show that, using standard Pfaffian techniques, one can obtain exact formulae for the p_i.

3. Classical probabilities

3.1. Pfaffian

The Pfaffian of a $(2n \times 2n)$ antisymmetric matrix M is defined as

$$\text{Pf } M = \sum_{\pi \in S_{2n}}{}' \epsilon(\pi) M_{\pi_1 \pi_2} M_{\pi_3 \pi_4} \cdots M_{\pi_{2n-1} \pi_{2n}}, \tag{19}$$

where $\epsilon(\pi)$ denotes the signature of a permutation π. The sum runs over all permutations of $\{1, 2, \ldots, 2n\}$ satisfying the constraints

$$\begin{aligned} &\pi_{2i-1} < \pi_{2i}, \qquad 1 < i < n \\ &\pi_{2i-1} < \pi_{2i+1}, \qquad 1 < i < n-1. \end{aligned} \tag{20}$$

A very important relation is

$$(\text{Pf } M)^2 = \det M. \tag{21}$$

It is especially useful because it allows us to compute the Pfaffian numerically in a time proportional to n^3 using standard determinant routines (and sometimes analytically).

3.2. Kasteleyn theory

The problem of enumerating dimer configurations on a planar lattice is a classic combinatorial problem, which was solved independently by Kasteleyn [19] and Temperley and Fisher [36]. We consider the case $t = 1$ for simplicity but the generalization to any t is straightforward. For any planar graph, the partition function (number of dimer coverings) is given by

$$\mathcal{Z} = |\text{Pf } \mathcal{K}|, \tag{22}$$

where $\mathcal{K}$ is an antisymmetric matrix constructed as follows. Putting arrows on all the links, a matrix element of $\mathcal{K}$ is

$$\mathcal{K}_{ij} = \begin{cases} +1 & \text{if the arrow points from } i \text{ to } j \\ -1 & \text{if the arrow points from } j \text{ to } i \\ 0 & \text{if } i \text{ and } j \text{ are not nearest neighbors.} \end{cases} \tag{23}$$

The Kasteleyn matrix must also satisfy the *clockwise-odd rule*: the product of the arrow orientations (± 1) around any elementary plaquette (running clockwise) has to be -1. Kasteleyn showed that (i) such a matrix $\mathcal{K}$ exists for any planar graph and (ii) it

J. Stat. Mech. (2012) P02003

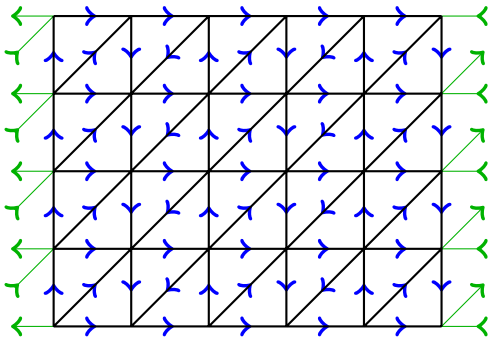

Figure 3. Kasteleyn orientation of the $(L_x = 6, L_y = 5)$ lattice (a weight t is given to 'diagonal' links). Blue arrows: orientation of the bonds. Green arrows: bonds present because of periodic boundary conditions along the x axis (see [37]). Their orientations are reversed compared to their 'bulk' counterparts.

ensures that all terms in the sum have the same sign (the signature of the permutation always compensates that of the product of matrix elements). It is immediate to check that (ii) implies equation (22).

A Kasteleyn matrix obeying equation (22) can also be found for cylindrical boundary conditions. An example for the triangular lattice with cylindrical boundary conditions[2] is shown in figure 3.

In the following we will demonstrate how each probability p_i can be computed as a determinant, taking the example of the cylinder geometry.

3.3. Classical probabilities

To find the probabilities of equation (16), we need to compute $\mathcal{Z}_i^A \mathcal{Z}_i^B$, which is the partition function restricted to dimer configurations compatible with the boundary spin configuration $|i\rangle = |\sigma_1, \ldots, \sigma_{L_x}\rangle$. It can be evaluated as the Pfaffian of a modified Kasteleyn matrix:

$$\mathcal{Z}_i^A \mathcal{Z}_i^B = \mathrm{Pf}\mathcal{K}^{(i)} \tag{24}$$

where $\mathcal{K}^{(i)}$ is deduced from $\mathcal{K}$ by removing the appropriate links in a simple way. If $\sigma_j = \uparrow$, a dimer emanating from the boundary site j has to be in A and we remove links in B emanating from site j. If $\sigma_j = \downarrow$ we remove links in A emanating from site j. See figure 4 for two examples, one with the boundary configuration $|i\rangle = |\Uparrow\downarrow\downarrow\uparrow\uparrow\downarrow\rangle$ and one with $|i\rangle = |\uparrow\uparrow\uparrow\uparrow\uparrow\uparrow\rangle$. The computation of any such probability apparently requires the ratio of two $L_xL_y \times L_xL_y$ determinants. However, using a known trick [20], the computation can be greatly simplified.

3.4. Perturbation theory for determinants in an infinite system

Following [20], p_i^2 may be written as

$$p_i^2 = \det(1 + \mathcal{K}^{-1}\mathcal{E}^{(i)}), \qquad \mathcal{E}^{(i)} = \mathcal{K}^{(i)} - \mathcal{K}. \tag{25}$$

[2] In the case of toroidal boundary conditions the situation is slightly more complicated, and the number of dimer coverings is given by a linear combination of four Pfaffians, see [37] for more details.

J. Stat. Mech. (2012) P02003

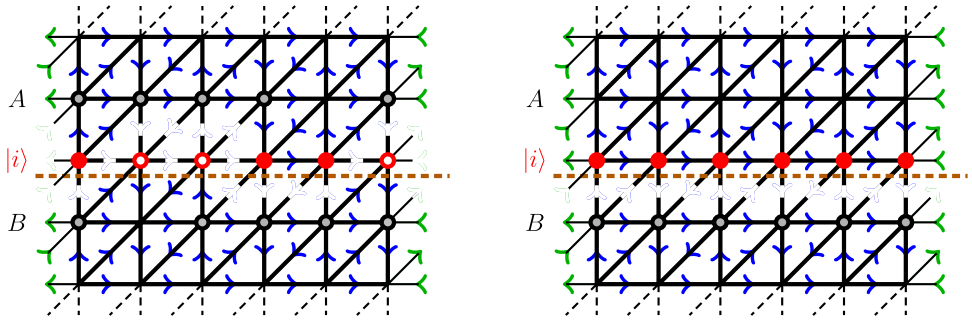

Figure 4. Two examples with $|i\rangle = |\uparrow\downarrow\downarrow\uparrow\uparrow\downarrow\rangle$ on the left, and $|i\rangle = |\uparrow\uparrow\uparrow\uparrow\uparrow\uparrow\rangle$ on the right. Filled red circle: boundary site occupied by a dimer in A (spin $\uparrow$). Empty red circle: boundary site occupied by a dimer in B (spin $\downarrow$). To ensure that a boundary site be occupied by a dimer in A (resp. B), all edges in B (resp. A) coming from this site have to be removed. Notice that after the removal, A and B are disconnected. Black circles filled in gray are sites which are connected to a boundary site through a link that has been removed. As explained in the text, the size of the determinant is given by the number of circles. p_i is therefore a 16×16 determinant for the configuration on the left and a 12×12 determinant for the configuration on the right.

The important point is that the matrix element $\mathcal{E}^{(i)}_{\mathbf{rr'}}$ is non-zero only if the link $\mathbf{r} \leftrightarrow \mathbf{r'}$ has been removed. Then, a matrix element of $\mathcal{K}^{-1}\mathcal{E}^{(i)}$ is

$$\left(\mathcal{K}^{-1}\mathcal{E}^{(i)}\right)_{\mathbf{rr'}} = \sum_{\mathbf{s}} \mathcal{K}^{-1}_{\mathbf{rs}} \mathcal{E}^{(i)}_{\mathbf{sr'}}. \tag{26}$$

It is non-zero only if $\mathbf{r'}$ is a site belonging to a removed link. We name these sites 'vicinity sites', and they of course depend on the boundary configuration $|i\rangle$. A boundary site is automatically a vicinity site, but the converse is not true, however. If we denote by E_i the set of vicinity sites and by n_i their number, $\mathcal{K}^{-1}\mathcal{E}^{(i)}$ is an $L_xL_y \times L_xL_y$ matrix, but only n_i columns are non-identically zero. Then, using the antisymmetry of the determinant, any cell with indices $\mathbf{r}$ and $\mathbf{r'}$ not both in E_i can be set to zero by appropriate linear combinations of rows and columns. Therefore, the determinant may be computed as its restriction to the sites in E_i:

$$p_i^2 = \det\left(\left(1 + \mathcal{K}^{-1}\mathcal{E}^{(i)}\right)_{|_{E_i}}\right). \tag{27}$$

This so-called 'perturbation theory for determinants' has been previously used in [20] to compute exactly the monomer–monomer correlation on the square lattice in the thermodynamic limit $(L, L_y \to \infty)$, and further extended in [16] to the triangular lattice. For computational purpose this is a huge simplification, because the size of the determinant has been reduced from L_xL_y to $n_i \sim \mathcal{O}(L_x)$, and the total system we are interested in can be infinite $(L_y \to \infty)$. In contrast also to the transfer matrix approach [18], this method allows us to treat any shape of boundary. This will be particularly useful while studying the geometry proposed by Kitaev and Preskill [6].

For this to work we also need to compute exactly certain matrix elements of the inverse Kasteleyn matrix $\mathcal{K}^{-1}$. This can be done using standard Fourier and integral techniques, see appendix A.

J. Stat. Mech. (2012) P02003

Let us now specify the case of the (infinitely long) cylinder geometry cut into two parts. An example of spin configuration is shown in figure 4, where boundary sites are represented by red circles (filled or empty, depending on the spin). Other vicinity sites are circles filled in gray. It is easy to check that $2L_x \leq n_i \leq 3L_x$ for all boundary configurations. Since there are *a priori* 2^{L_x} boundary configurations and each probability is of complexity $\sim n_i^3$, the Rényi entropy can be evaluated in a time $\sim L_x^3 \times 2^{L_x}$. This allow us to go to relatively large system sizes of order $L_x \sim 30$.

4. Results for the infinite cylinder

When the height L_y is infinite, the entropies S_n only depend on the perimeter $L_x = L$. As usual, the leading term is non-universal and scales with L, and we are interested in the first subleading contribution s_n:

$$S_n(L) \simeq \alpha_n L + s_n + \mathrm{o}(1). \tag{28}$$

4.1. Topological entanglement entropy and Rényi index

For gapped topological wavefunctions, the subleading constant s_1 in the von Neumann entropy has been shown to be related to the content of the phase in terms of fractionalized particles, and to the total quantum dimension D in particular [6, 7]: $s_1 = -\ln(D)$. In the original works the subleading constant s_1 was extracted by combining the entropies of different subsystems in a planar geometry. We show here that the subleading term can be extracted in a—somewhat simpler—cylinder geometry (see also [10]).

For $t > 0$ the present dimer wavefunctions realize the simplest topological phase, the so-called $\mathbb{Z}_2$ liquid with quantum dimension $D = 2$. One therefore expects to have $s_1 = -\ln 2$ in the whole topological phase. So far, this has only been checked numerically at $t = 1$ [11]. In addition, [21] argues that this topological entanglement entropy is independent of the Rényi index n. We present here some results for infinitely high cylinders for various values of t and n, which support this result. The convergence to the topological entropy is exponentially fast, as can be seen in figure 5. For generic values of t and n, this allows us to get this constant with a very high accuracy: for example, at $t = 1$ our best estimate is $|s_1(t = 1) + \ln 2| \simeq 10^{-9}$. It is widely believed that in massive phases the topological entropies (subleading terms) are independent of short-range correlations, but this is not *proven*. The present results, which strongly indicate that $s_n = -\ln(2)$ for any $t > 0$, therefore brings some additional support to the robustness of topological entropies. In general finite-size effects get larger when increasing n at fixed t, and it is more advisable to numerically study low-n Rényi entropies. However, as is shown in B.2, the calculation for $n \to \infty$ simplifies greatly and the result $s_\infty(t > 0) = -\ln 2$ can even be obtained rigorously. We further discuss this result in section 4.5. At fixed n the convergence is also less clear when t is small since the correlation length $\xi(t)$ diverges when approaching $t = 0$ and the finite-size effects become very important when $L \gtrsim \xi(t)$. Still, the curve $s_n(t > 0)$ approaches $-\ln 2$ when $L \to \infty$. The data plotted in figure 6 are indeed compatible with $s_n(t) = -\ln 2$ for all $n = 0.5, 1, 2$ and $t > 0$. The scaling close to $t = 0$ will be discussed later in section 4.3.

J. Stat. Mech. (2012) P02003

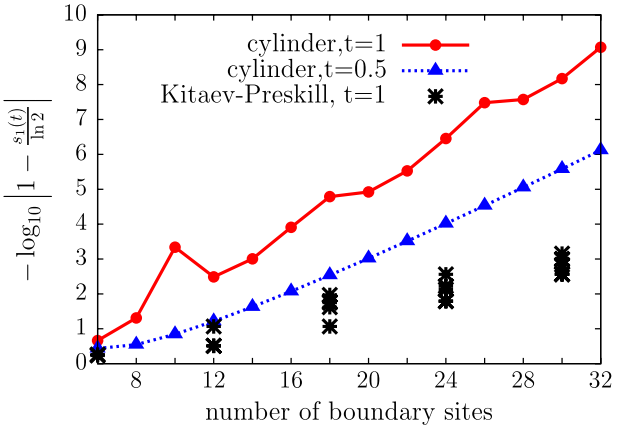

Figure 5. Number of correct digits in the numerical estimate of the topological constant, as a function of the number of boundary sites. For the cylinder geometry we show the data for $t = 1$ (red circles) and $t = 0.5$ (blue triangles). The number of boundary sites is just L in this case and the estimate is obtained by a fit to $aL + s_1$ for two even consecutive values of L. The convergence to the correct value is exponentially fast, with an effective correlation length close to the dimer–dimer correlation length (which can have an imaginary part [16, 17], hence the oscillations we observe). For comparison we also show the data in the Kitaev–Preskill geometry, slightly anticipating section 6.

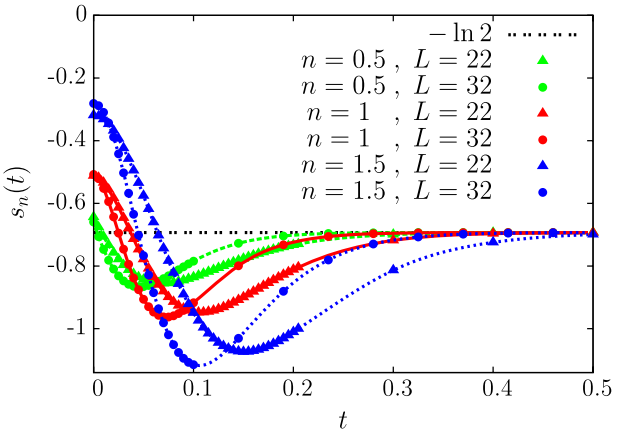

Figure 6. Subleading constants $s_n(t)$ for three different values of the Rényi parameter ($n = 0.5, 1, 1.5$). For each t and n, $s_n(t)$ is extracted from $S_n(L)$ using two consecutive even values of L (up to $L = 32$). In the thermodynamic limit the results are expected to converge to $s_n(t) = -\ln 2$ for all $n > 0$ and $t > 0$.

4.2. Thermodynamical entropy

The behavior for large values of the Rényi index n is displayed in figure 8 (triangular dots). Although it is roughly constant and close to $-\ln(2)$, due to the finite size of the system there are some visible deviations for $n \gtrsim 3$. This is even more visible if we consider

J. Stat. Mech. (2012) P02003

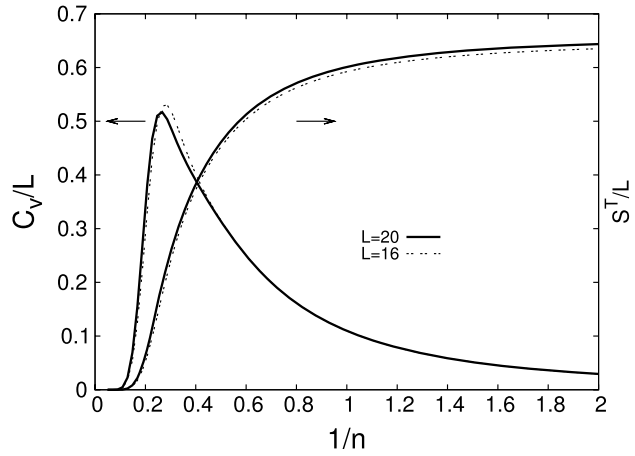

Figure 7. Thermodynamic entropy per site S_n^{T}/L (monotonically increasing, right axis) and its associated 'specific heat' (peaked at $n \simeq 0.25$, left axis) $C_v = -n\,\mathrm{d}S^{\mathrm{T}}/\mathrm{d}n$. Fugacity $t = 1$.

a slightly different entropy, S_n^{T}, defined as

$$S_n^{\mathrm{T}} = (1 - \partial_n) \ln (Z_n) \tag{29}$$

$$Z_n = \sum_i p_i^n \tag{30}$$

which can also be written as the Shannon entropy associated with the normalized probabilities $\tilde{p}_i$:

$$S_n^{\mathrm{T}} = -\sum_i \tilde{p}_i \ln(\tilde{p}_i) \qquad \text{with } \tilde{p}_i = \frac{p_i^n}{Z_n}. \tag{31}$$

Both entropies match at $n = 1$ ($S_{n=1}^{\mathrm{T}} = S_{n=1}$) and are simply related otherwise: $S_n^{\mathrm{T}} = (1 - n\partial_n)((1 - n)S_n)$. The 'thermodynamic' entropy S^{T} also has a leading term $\mathcal{O}(L)$ and a subleading term, s_n^{T}. The extensive (and non-universal) part is plotted in figure 7 as a function of the 'temperature' $1/n$. To stress the similarity with the usual statistical mechanics, we also plotted the associated 'specific heat' defined as a derivative of S^{T}: $C_v = -n(\mathrm{d}S^{\mathrm{T}}/\mathrm{d}n)$.

The subleading term s_n^{T} is plotted in figure 8 (crosses). It is very close to $-\ln(2)$ at small n, but goes to $s^{\mathrm{T}} = 0$ when $n \to \infty$. This is indeed expected since the thermodynamic entropy $S_{n=\infty}^{\mathrm{T}}$—which corresponds to zero 'temperature'—is equal to the log of the degeneracy of the configuration with the highest probability, which is non-degenerate in our case. However, the crossover from $-\ln(2)$ to 0 takes place at values of n which are larger and larger when $L \to \infty$. This can be checked in the inset of figure 8, where the numerical data appear to be correctly fitted by

$$s_{n \gg \ln(L)}^{\mathrm{T}} \sim L^2 \exp(-n\Delta) \tag{32}$$

$$s_{n \ll \ln(L)}^{\mathrm{T}} \sim -\ln(2) \tag{33}$$

J. Stat. Mech. (2012) P02003

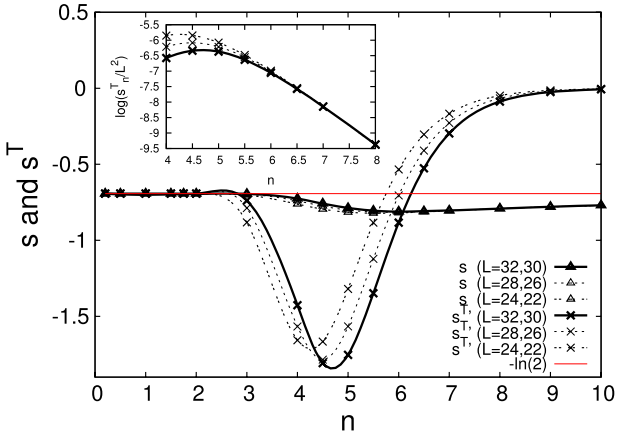

Figure 8. Large n behavior of the subleading constant $s_n(t=1)$ of the Rényi entropy, and $s_n^{\mathrm{T}}(t=1)$, the subleading constant of the thermodynamical entropy. They both give $-\ln(2)$ for small n, but differ for large n. This is a finite-size effect: as shown in the inset, $s^{\mathrm{T}} \sim L^2 \exp(-\Delta n)$ for large n. We thus have $s \simeq s^{\mathrm{T}} = \simeq -\ln(2)$ up to $n \sim \ln(L)$.

where $\Delta \simeq 1.32$ is the entanglement gap at $t=1$. We finally note that the calculation of $p_{\max}$ given in appendix B.2 proves rigorously that $\lim_{L\to\infty} \lim_{n\to\infty} s_n = -\ln(2)$ and $\lim_{L\to\infty} \lim_{n\to\infty} s_n^{\mathrm{T}} = 0$.

4.3. Scaling when $t \to 0$ and $L \to \infty$ with fixed $L \cdot t$

The critical point $t=0$ has already been studied [18, 31] and is known to give

$$s_n(0) = \begin{cases} \ln R - \dfrac{\ln n}{2(n-1)}, & 0 < n \leq 1 \\ \dfrac{n}{n-1} \ln R, & n > 1 \end{cases} \tag{34}$$

$$s_n^{\mathrm{T}}(0) = \begin{cases} \ln\left(\sqrt{n} R\right) - \frac{1}{2}, & 0 < n \leq 1 \\ 0, & n > 1, \end{cases} \tag{35}$$

where the compactification radius is $R = 1$ (free fermions) for the present dimer wavefunctions, but could be tuned by adding some dimer–dimer interactions [34].

The correlation length $\xi(t)$ diverges as $\xi(t) \sim t^{-1}$ when $t \ll 1$ [16]. In figure 9 we plot the subleading constant $s_n(t, L)$ as a function of $L \cdot t \simeq L/\xi(t)$. It appears that, for a given value of n, the data curves corresponding to different values of t and L approximately collapse onto each other. This shows that, when the system size L is much bigger than the correlation length $\xi(t) \sim t^{-1}$, we find the correct topological entanglement entropy $s_n = -\ln(2)$. On the other hand, when L is of the same order of magnitude than $\xi(t)$ (and much larger than the lattice spacing), s_n turns out to be some non-trivial function of n and $L \cdot t$. When $L \cdot t \to 0$ the system effectively behaves as a critical system of dimers on a square lattice and s_n converges to equation (34), as expected.

J. Stat. Mech. (2012) P02003

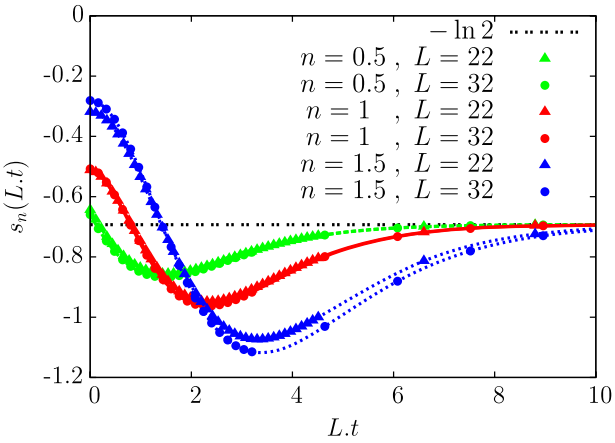

Figure 9. Subleading constants s_n as a function of $t \times L$. For each value of n, the data corresponding to different values of t and L appear to be well described by a function of $t \times L$ only.

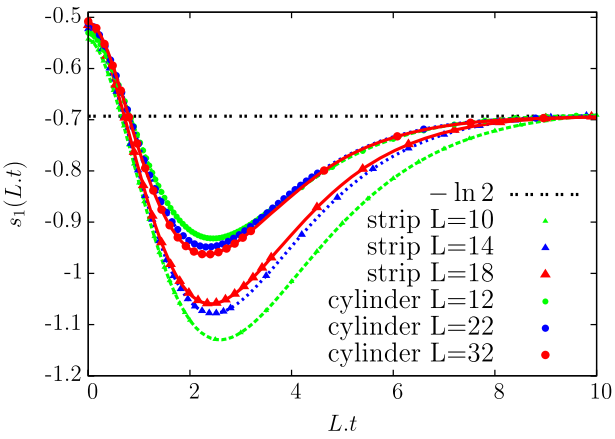

Figure 10. Subleading constants for the entanglement entropy calculated numerically in two geometries: half-infinite cylinder and zig-zag strip (see text).

4.4. Entropy of a zig-zag line

As explained in section 2.3, the eigenvalues of the RDM of a half-infinite cylinder are the classical probabilities of the 'spin' configurations $|i\rangle = |\sigma_1, \sigma_2, \ldots, \sigma_L\rangle$. But one may also consider a zig-zag line and the probabilities p_α of the dimer configurations on that line. The 'spins' are now replaced by the dimer occupancies (say, 0 or 1) of the zig-zag bonds. These probabilities can be computed using exactly the same perturbed-Pfaffian method as before. However, in terms of entanglement, the entropy we compute is that of the 'zig-zag' chain shown on the right of figure 10. Although the probabilities are computed in a very similar way, this calculation does not describe the entanglement of a two-dimensional subsystem, but that of a one-dimensional line winding around the cylinder.

The associated entropies, already considered in [11], have a leading term proportional to L and a subleading contribution of order $\mathcal{O}(L^0)$. The results, plotted in figure 10, show that the subleading constant s_1 has a dependence on t and system size L which is very

J. Stat. Mech. (2012) P02003

similar to that of the half-cylinder entropy. It is possible that, as a function of $L \cdot t$, the zig-zag line and half-infinite cylinder converge to the same curves for sufficiently large L. In any case, the zig-zag results clearly converge to $-\ln(2)$ in the thermodynamic limit for $t > 0$.

One may ask if the zig-zag entropy would also give access to the quantum dimension for a *general* topologically ordered wavefunction (not of RK type, and even not based on dimers). We believe that it is *not* the case. The present dimer RK states enjoy a special property: once the dimer occupancies are fixed along the zig-zag chain, the upper and lower half-cylinders are completely decoupled. For this reason, the entropy of the zig-zag chain is very close to that of a half-cylinder. This would not hold for more generic states and a *thick* strip (sufficiently large compared to the correlation length) would probably be required to access the quantum dimension in general.

4.5. Infinite Rényi and bipartite fidelity

As already emphasized, the infinite-n Rényi limit selects the largest eigenvalue of the RDM, which is the probability of the most likely configuration in the dimer language:

$$S_\infty = -\ln p_{\max}. \tag{36}$$

For the cylinder geometry the corresponding boundary configuration $|i_{\max}\rangle$ is particularly simple (see figure 4 for a graphical representation):

$$|i_{\max}\rangle = |\uparrow\uparrow\cdots\uparrow\rangle, \tag{37}$$

and $p_{\max}$ can be expressed as a ratio of simple partition functions:

$$p_{\max} = \lim_{L_y\to\infty} \frac{[Z_{\rm cyl}(L_x, L_y/2)]^2}{Z_{\rm cyl}(L_x, L_y)}, \tag{38}$$

where $Z_{\rm cyl}(L, h)$ is the partition function for dimers on a finite cylinder of length L and height h. As detailed in appendix B, we then find the following expression for S_∞:

$$S_\infty = -\sum_{k=(2m-1)\pi/L}^{1\le m\le L/2} \ln\left(\frac{1}{2} + \frac{1}{2}\frac{\sin^2 k - t\cos k}{\sqrt{t^2+\sin^2 k+\sin^4 k}}\right), \tag{39}$$

from which one can extract the subleading constant:

$$s_\infty(t) = \begin{cases} 0, & t = 0 \\ -\ln 2, & t > 0. \end{cases} \tag{40}$$

This result has already been mentioned in section 4.1. The entropy S_∞ can also be considered from a different point of view. $|RK\rangle$ is the ground state of the Rokhsar–Kivelson Hamiltonian and lives on a cylinder of length L and height h. This Hamiltonian may be written as

$$H = H_{A\cup B} = H_A + H_B + H_{A,B}^{(\rm int)}, \tag{41}$$

where H_A (resp. H_B) is the Rokhsar–Kivelson Hamiltonian restricted to sites in A (resp. B). We have $[H_A, H_B] = 0$ and $H_{A,B}^{(\rm int)}$ contains all the interactions between A and B. If we denote by $|A\rangle$ (resp. $|B\rangle$) the ground state of H_A (resp. H_B), $|A\otimes B\rangle = |A\rangle\otimes|B\rangle$ the

J. Stat. Mech. (2012) P02003

ground state of $H_A + H_B$ and by $|A \cup B\rangle = |RK\rangle$ the ground state of $H_{A\cup B}$, then $p_{\max}$ can be reformulated as

$$p_{\max} = |\langle A \cup B | A \otimes B\rangle|^2. \tag{42}$$

Taking minus the logarithm we get

$$S_\infty = -\ln |\langle A \cup B | A \otimes B\rangle|^2. \tag{43}$$

The rhs of equation (43) has been studied in [38] under the name 'logarithmic bipartite fidelity' (LBF). The (infinite) Rényi entanglement entropy and the LBF are *a priori* not related, but we find that they are simply equal for this particular RK wavefunction. In other words, performing a Schmidt decomposition on the total wavefunction $|A \cup B\rangle$, the Schmidt state with the highest Schmidt value is nothing but the ground state of $H_A + H_B$, the RK Hamiltonian, where all interactions between A and B were switched off.

However, this relation does not hold exactly in general. For instance, in the Kitaev–Preskill or Levin–Wen geometry the boundaries are not straight and in that case the boundary dimer configuration $|i_{\max}\rangle$ is not as simple as for the cylinder. Still, as pointed out in [38], the equivalence between the LBF and S_∞ can hold for some more complex topological states such as the string-net states constructed by Levin and Wen [7]. We expect that for a generic (i.e. non-RK) gapped state, the subleading term in the LBF and S_∞ should be the same in the thermodynamic limit (although, due to some mismatch at short distances, the extensive terms will differ). The argument is as follows: starting from a string-net state where the correspondence works, we adiabatically modify the wavefunction towards the state we are interested in (without closing the gap). Doing so it is natural to expect that only the short-distance properties of the entanglement will be modified (hence the $\sim L$ term) but not the subleading constant s_∞, which is expected to be free from the contribution of local correlations. Although the robustness to changes in local correlations is not proven in general, we provide in appendix B a rigorous proof that the subleading term s_∞ is equal to $-\ln 2$ in the whole massive phase of the model ($t > 0$).

4.6. Entanglement gap and entanglement spectrum

The *spectrum* of the RDM contains some rich information about the system. Looking at such spectra has been particularly fruitful in the context of the quantum Hall effect (QHE), where the entanglement spectrum was shown [39] to reflect some properties of the chiral gapless excitations which can propagate along an edge [40]. With the RK wavefunctions the RDM eigenvalues are simple classical probabilities and we thus have a relatively easy access to the entanglement spectra of large systems.

Such spectra shown in figures 11–12, where the probabilities p_i have been converted to 'energies': $E_i = -\ln(p_i/p_{\max})$. The first observation is that these spectra have a unique ground state and a gap $\Delta = E_1$ to the first 'excitation'. This is true not only in the $\mathbb{Z}_2$ liquid ($t > 0$) but also for the critical RK wavefunction at $t = 0$. So, contrary to the QHE where a well-defined set of low-energy levels are separated from the rest [39, 41], there is no apparent low-energy structure in the spectrum but a single 'ground state'. One could have naively expected the entanglement gap to close when reaching the critical point at $t = 0$, but this is not the case. As can be seen in figure 12, the entanglement

J. Stat. Mech. (2012) P02003

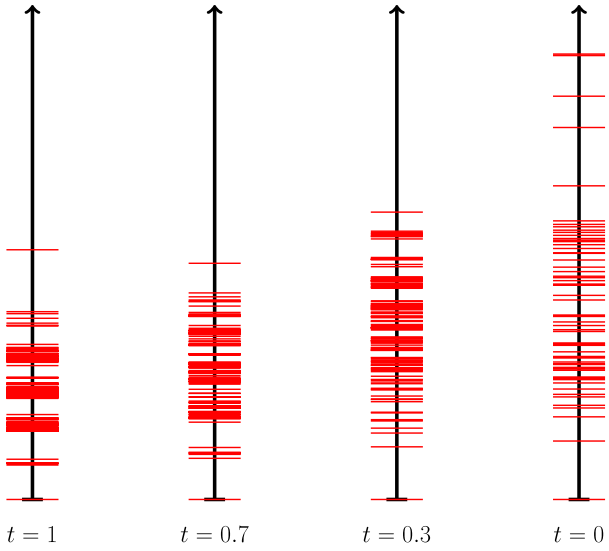

Figure 11. Entanglement spectrum for $L = 12$ and for $t = 1, 0.7, 0.3$ and 0 from left to right.

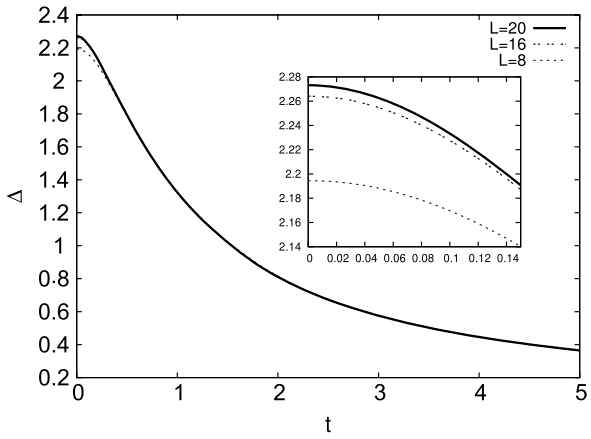

Figure 12. Entanglement gap as a function of t. It is maximum at $t = 0$ (square lattice) and decreases slowly to zero when $t \to \infty$. Except very close to $t = 0$ (inset) the curves for $L = 16$ and 20 are practically indistinguishable on the scale of the figure, signaling negligible finite-size effects.

gap remains finite all the way from $t = 0$ to 1 (it vanishes only at $t = \infty$). We have, for instance, $\Delta = 1.323\,14$ at $t = 1$ (exponentially fast convergence as a function of L) and $\Delta = 2\ln(\pi) \simeq 2.29$ at $t = 0$.[3] A possible interpretation is the following: the entanglement spectrum is indeed related to the spectrum of the excitations that would propagate along

[3] This analytical result for Δ in the thermodynamic limit of the square lattice can be obtained by noticing that the configuration with the highest probability is $|\uparrow\uparrow\cdots\uparrow\rangle$ while the next configuration has two consecutive flipped spins $|\uparrow\uparrow\downarrow\downarrow\uparrow\cdots\rangle$. One can check that, for $t = 0$, the ratio $p_1/p_{\max}$ of these two probabilities is nothing but the square of the probability for a bond located at the edge of a semi-infinite square lattice to be occupied by a dimer. The latter probability has been computed in [20] and is equal to $1/\pi$, which gives $\Delta = -\ln(p_1/p_{\max}) = 2\ln(\pi)$.

J. Stat. Mech. (2012) P02003

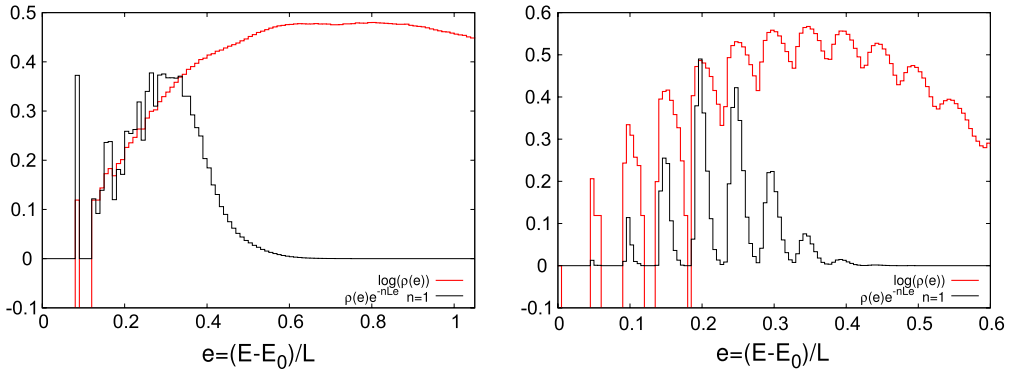

Figure 13. Logarithm of the density of states ρ associated with the entanglement spectrum of a half-infinite cylinder as a function of the 'energy' per site $e = (E - E_0)/L$ (arbitrary units). Top: $t = 0$ (square lattice), bottom: $t = 1$ (triangular lattice). To display the energy range which contributes to the von Neumann entropy S_1, the probability distribution $p(e) \sim \rho(e)\exp(-neL)$ is also plotted for $n = 1$. System size: $L = 28$.

an edge. However, in the dimer systems we consider, there are no gapless edge excitations, even though the bulk may be gapless for $t = 0$.

In the thermodynamic limit, it is possible to adopt a microcanonical point of view where the entropy $S(e)$ is simply related to the density of states:

$$S(e) = \ln(\rho(e)) \tag{44}$$

with

$$\rho(e) = \sum_i \delta(e - E_i/L). \tag{45}$$

Knowing the entropy $S(e)$ from the spectrum, the energy $e(n)$ can be obtained as a function of the Rényi index n by inverting

$$\frac{\mathrm{d}S}{\mathrm{d}e} = n(e). \tag{46}$$

The entropy S_n is then obtained as

$$S_n = \ln(\rho(e(n))). \tag{47}$$

We conclude that, for sufficiently large L, the entropy only depends on the density of states at some high energy $E = L \cdot e(n)$ in the spectrum.

The microcanonical entropy per site $S(e)/L$ is displayed in figure 13 for the triangular and square lattice (half-infinite cylinders with $L = 28$). Some (finite-size) oscillations are visible in the triangular case and can be interpreted as the successive energy 'bands' corresponding to $0, 2, 4, \ldots$, spin flips in the boundary state. These oscillations will be smeared out in larger systems, however.

J. Stat. Mech. (2012) P02003

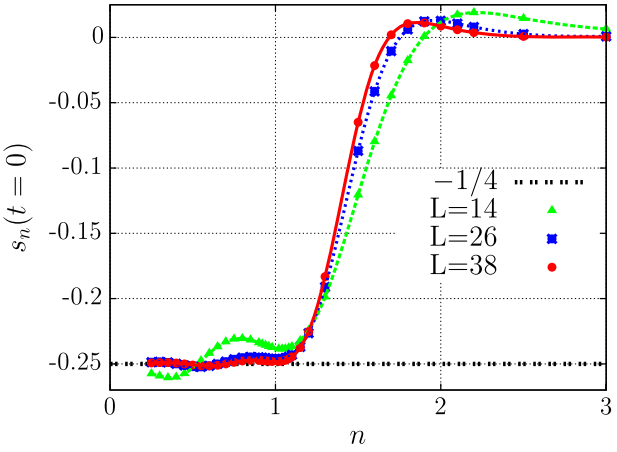

Figure 14. Coefficient of the logarithmic term in the Rényi entropy for the strip geometry, as a function of the Rényi parameter n. This term is extracted from a fit $S_n = aL + b\ln L + c + d/L$ on the systems sizes $L-6, L-4, L-2, L$. Three values $L = 14, 26$ and 38 are shown. The data is consistent with the CFT results. For $n \leq n_c = 1$, the logarithmic contribution is approximately ~ -0.25 (see [18]). For $n > n_c$ it is close to zero as discussed in [31].

5. Long strip geometry

The triangular lattice can also be constructed with open boundary conditions in the x direction. The geometry is no longer that of a cylinder but a long strip. In such a situation the leading term in the entropy is still proportional to the width of the strip $L_x = L$, but the sharp corners also contribute to the subleading constant and it is not possible to extract the topological entropy for $t > 0$. The critical case is more interesting, because the first subleading correction is now a logarithm of the width. The latter was originally predicted to be $-\ln(L)/4$ by Fradkin and More [25] (an application of the Cardy–Peschel formula [42] which describes the universal logarithmic contribution of sharp corners to the free energy in a CFT). These terms have recently been observed numerically in the closely related Shannon entropy of open critical spin chains [30, 31].

In figure 14 we show the coefficient of the $\ln(L)$ term as a function of the Rényi index n for the square lattice dimer wavefunction with open boundary conditions. The prediction of Fradkin and More, $-\frac{1}{4}$, is verified up to $n \simeq 1$. For larger values of n the logarithmic term vanishes. This is a manifestation of the boundary phase transition discussed in [31]. Indeed, above n_c the compactness of the height field can no longer be ignored since a vertex operator $\cos(dh/r)$ (with d an integer) becomes relevant at the boundary. The value of d can be obtained by looking at the microscopic configuration $|i_{\max}\rangle$ with maximal probability. Contrary to the case of the XXZ chain, this configuration is non-degenerate: $d = 1$ in the notation of [31]. Since the Luttinger parameter R is equal to 1 for the dimer problem (free fermions), the analysis of [31] immediately gives $n_c = d^2/R = 1$, in agreement with the present numerics. Above n_c the universal contribution to the entropy is that of a single 'flat' height configuration. As in the XXZ chain, this flat configuration does not correspond to a simple Dirichlet boundary condition around A in the continuum

J. Stat. Mech. (2012) P02003

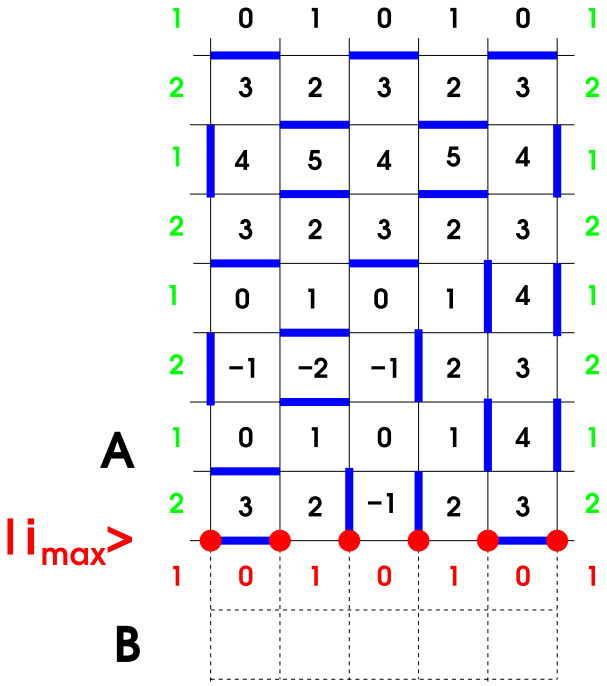

Figure 15. Configuration $|i_{\max}\rangle$ with the maximal probability on the square lattice and a compatible dimer covering of the rectangular region A. The microscopic heights are indicated in units of $\frac{1}{2}\pi r$. When turning clockwise around a site of the even (resp. odd) sublattice the height changes by $+1$ (resp. -1) when crossing an empty bond and changes by -3 (resp $+3$) when crossing a dimer. The lower horizontal boundary of A has a coarse-grained height which is 'flat', with an average height equal to $\frac{1}{2}(0+1) = \frac{1}{2}$ (red). The vertical boundaries have a coarse-grained height equal to $\frac{1}{2}(1+2) = \frac{3}{2}$ (green). In the continuum limit there is a height shift $\delta = \pm\frac{1}{2}\pi r$ at each corner of A.

limit. Indeed, the (coarse-grained) height is shifted by an amount $\delta = \frac{1}{2}\pi r$ with respect to the vertical boundaries of the lattice (see figure 15). As in the XXZ chain situation, this height shift produces a logarithmic term which exactly compensate the logarithmic terms coming from the Cardy–Peschel angles, hence the absence of a logarithm in the Rényi entropy when $n \geq n_c = 1$.

6. Kitaev–Preskill construction

As discussed in section 4 the cylinder geometry allows us to extract the subleading entropy term in a rather straightforward way, by a simple fit of $S_n(L)$ on (at least) two system sizes. However, the original proposals [7, 6] were to extract the topological entanglement entropy from a single and large planar system. There, the subsystems on which the entanglement entropy are computed cannot have a straight boundary and necessarily have corners, etc. These corners (as well as the curvature) also contribute to the entanglement entropy by a (non-universal) amount of order one and therefore need to be subtracted.

J. Stat. Mech. (2012) P02003

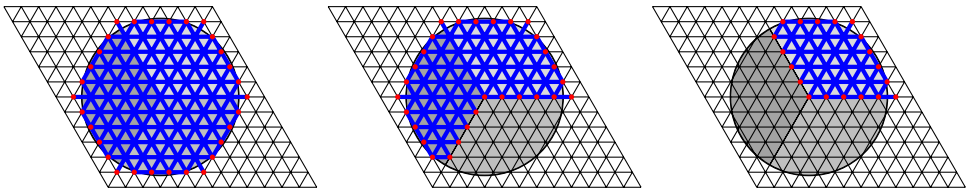

Figure 16. Geometries required for the computation of $S_n^{(ABC)}$, $S_n^{(AB)}$ and $S_n^{(A)}$ at radius $\rho = 4.5$. They have $N_b = 30$, 29 and 19 boundary sites (in red), respectively.

The subtraction scheme proposed by Kitaev and Preskill [6] is based on the following combination of entropies (see figure 16):

$$S_n^{\text{topo}} = S_n^{(ABC)} - S_n^{(AB)} - S_n^{(BC)} - S_n^{(AC)} + S_n^{(A)} + S_n^{(B)} + S_n^{(C)}. \tag{48}$$

The first numerical implementation of this subtraction idea was done in the RK dimer wavefunction at $t = 1$ and $n = 1$ [25]. Some other recent works investigated the $n = 2$ case using quantum Monte Carlo on a Bose–Hubbard model [43] and variational quantum Monte Carlo on projected spin liquid wavefunctions [44]. Here we extend the results of [25] on dimer RK wavefunctions for several values of t and n, and with finite areas A, B and C embedded in an *infinite* plane. The results are shown in figure 17. Provided t is not too small (i.e. the dimer–dimer correlation length is not too large), the Kitaev–Preskill construction gives an entropy constant equal to $-\ln(2)$ with high precision, as expected. Still, for the same numerical effort (boundary length), the convergence turns out to be slower than with the cylinder geometry (see figure 5).

Equation (48) was originally designed to probe a *massive* wavefunction, but it is also natural to consider the limit $t \to 0$ where the wavefunction becomes critical (and restricting to $n < n_c$ for simplicity).

Each term in equation (48) corresponds to a subsystem $\Omega = ABC, AB, \ldots$, which is topologically equivalent to a disc, but possibly with some sharp corners. For each such subsystem, we wish to use a formula derived in [31]:

$$S_n(\Omega) = \frac{1}{1-n}\left[\ln\left(\frac{\mathcal{Z}_{n\kappa}}{\mathcal{Z}^{\text{D}}_{n\kappa}}\right) - n\ln\left(\frac{\mathcal{Z}_{\kappa}}{\mathcal{Z}^{\text{D}}_{\kappa}}\right)\right], \tag{49}$$

where $\mathcal{Z}$ is a free-field partition function on the whole system and $\mathcal{Z}^{\text{D}}$ is the partition function with Dirichlet boundary condition imposed at the boundary of Ω (thus disconnecting Ω and $\bar{\Omega}$). κ is the bare stiffness and the first term should be evaluated with a modified stiffness $\kappa' = n\kappa$.[4]

By construction, the non-universal contributions proportional to the boundary length will drop out of the KP combination. Next, we consider the logarithmically divergent terms which come from the sharp corner contributions to the free energies. Each corner with interior angle α gives a contribution $F(\alpha) = \frac{1}{24}(\alpha/\pi - \pi/\alpha)\ln(L/l_0)$ to the free

[4] This formula was originally derived in the case where Ω is a half-infinite cylinder, but the argument probably applies to the present geometries as well.

J. Stat. Mech. (2012) P02003

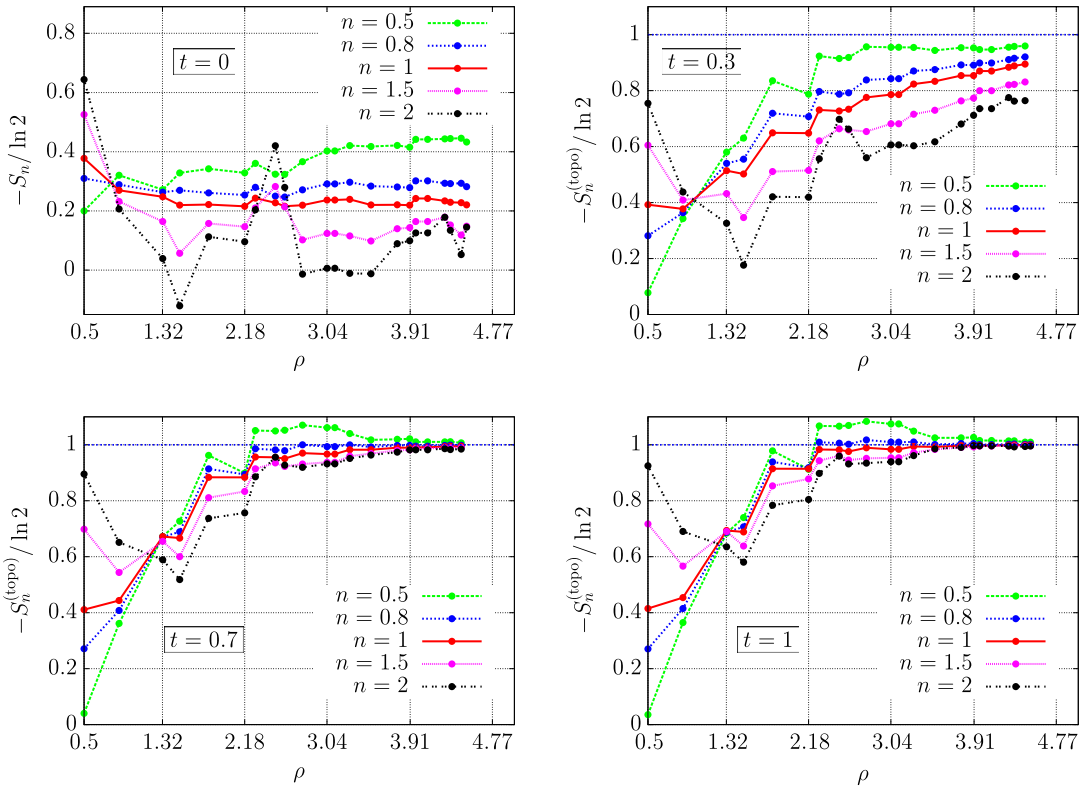

Figure 17. Top left: critical case $t = 0$. Top right: $t = 0.3$. Bottom left: $t = 0.7$. Bottom right: $t = 1$. In each case, $-S_n^{\mathrm{topo}} / \ln 2$ is shown for $n = 0.5, 0.8, 1, 1.5$ and 2 as a function of the radius ρ.

energy, where L is the typical scale of the boundary and l_0 some microscopic cutoff [42]. To apply equation (49) what needs to be computed is the free energy difference between that of the whole system and that where Ω and $\bar{\Omega}$ have been disconnected (Dirichlet boundary condition). So, in the disconnected term, a sharp corner of angle α in Ω will also contribute as a sharp corner of angle $2\pi - \alpha$ (in $\bar{\Omega}$). The contribution to S_n is thus $\delta S_n = F(\alpha) + F(2\pi - \alpha) = \frac{1}{24}(2 - (\pi/\alpha) - \pi/(2\pi - \alpha)) \ln(L/l_0)$, which is by construction symmetric under the exchange $\alpha \leftrightarrow 2\pi - \alpha$. Then it is easy to check that, in the spatial decomposition implied by (48), each angle appearing in some $+S_\Omega$ will cancel out with another one (with the same angle or its complement) in $-S_{\Omega'}$.

However, as already mentioned in [43], this is only true for the leading (logarithmically divergent) part, because there is no simple reason why the microscopic length scales l_0 should all be the same. We thus expect some constant (non-divergent) and non-universal contribution to the entropy when $t = 0$.

References [25, 26] mentioned that the entanglement entropy of a disc Ω of radius R embedded in a larger disc $\bar{\Omega}$ of radius L could have a (very slowly) diverging term $\sim \ln(\ln(L/R))$ for a critical RK wavefunction. However, in the lattice (dimer) version of the RK state we consider, it is easy to show that the entropy must be finite when $L \to \infty$ while keeping R fixed. The argument is as follows: the (von Neumann) entropy S_1 of a

J. Stat. Mech. (2012) P02003

subsystem can be expressed using the probabilities p_i of its boundary configurations:

$$S_1 = -\sum_{i=1}^{N} p_i \ln(p_i) \tag{50}$$

where N is the number of possible microscopic configurations at the boundary of Ω. If the boundary has a finite length $\sim R$, N must be finite with $\ln N \sim R$. As a consequence, since the entropy is bounded by $\ln N$, we have $S_1 \lesssim R$. In other words, the entanglement entropy cannot exceed the boundary law for RK states. This bound does not involve the size of the outer system $\bar{\Omega}$ and none of the entropies appearing in equation (48) can diverge when taking the outer system to its thermodynamic limit. Why the argument of [25] does not apply to this quantity in lattice RK states is, however, unclear to us. But in any case $S_{\text{topo}}(R)$ cannot diverge when taking $L \to \infty$ at fixed R, whatever the lattice RK state provided it has a finite number of states per site. This is indeed confirmed by our numerical estimations of $S_{\text{topo}}(R)$ which are performed directly in the thermodynamic limit $L = \infty$ and which gives finite values for finite values R. Although the system sizes (R) are too small to observe the true large-R behavior for $t = 0$ (square lattice), the argument above concerning the corner contribution indicates that it is very likely a non-universal number.

7. Summary and conclusions

Thanks to some extensive use of the Pfaffian solution of the classical (2d) dimer model, we have performed exact calculations of the entanglement entropy and entanglement spectra of some dimer RK states on large subsystems. Using the cylinder and the Kitaev–Preskill geometries we recovered the topological entanglement entropy of the $\mathbb{Z}_2$ phase, $-\ln(2)$, with high accuracy. As expected, this value not only holds for the triangular lattice RK wavefunction, but is in fact independent of the fugacity $t > 0$. We also analyzed the scaling close to the critical point at $t = 0$, as well as the behavior for large values of the Rényi index n. In particular, we proved for $n \to \infty$ that the subleading entropy constant is $-\ln(2)$. Thanks to its translation-invariant boundary, the cylinder geometry gives smaller finite-size effects and therefore a much more precise estimation of the topological entanglement entropy than the KP set-up (for a given length of the subsystem boundary). For this reason, it may be preferred in future numerical studies (exact diagonalization or quantum Monte Carlo) looking for topological ground states in realistic lattice models.

The entanglement spectra were also computed in the cylinder geometry, and the presence of a unique ground state and a finite gap (whatever the fugacity) showed that for these states, contrary to naive expectations, the topological (or critical) nature of the phase is not apparent in the low-energy part of the entanglement spectrum. Simpler $\mathbb{Z}_2$ wavefunctions such as that of the Toric Code [13] (or that of [14]) do not allow us to learn much about the structure of the entanglement spectrum. Indeed, in those states with vanishing correlation length all the non-zero eigenvalues of the reduced density matrix are exactly degenerate (no n dependence of the Rényi entropy). From this point of view, the dimer states we consider offer an interesting compromise between the possibility to do exact calculations on large systems and a non-trivial entanglement spectrum. Extending these calculations to other states with richer topological structure, like string-net wavefunctions [45], could be a promising direction of research.

J. Stat. Mech. (2012) P02003

Appendix A. Green function elements for an infinite cylinder

A.1. Diagonalization of the Kasteleyn matrix

We wish to diagonalize the Kasteleyn matrix by a Fourier transform for $L_y \to \infty$. To do so we must distinguish between two sublattices (see figure 3):

$$\mathcal{L}_0 = \{(2x\mathbf{u_x} + y\mathbf{u_y}) | 0 \leq x < L_x | 2, 0 \leq y < L_y\} \tag{A.1}$$

$$\mathcal{L}_1 = \{(2x+1)\mathbf{u_x} + y\mathbf{u_y} | 0 \leq x < L_x/2, 0 \leq y < L_y\}. \tag{A.2}$$

We denote by $N = L_x L_y$ the number of sites. Then we define a new basis:

$$|\mathbf{k}, 0\rangle = \frac{1}{\sqrt{N/2}} \sum_{\mathbf{r}_0 \in \mathcal{L}_0} \mathrm{e}^{-\mathrm{i}\mathbf{k}\cdot\mathbf{r}_0} |\mathbf{r}_0\rangle \tag{A.3}$$

$$|\mathbf{k}, 1\rangle = \frac{1}{\sqrt{N/2}} \sum_{\mathbf{r}_1 \in \mathcal{L}_1} \mathrm{e}^{-\mathrm{i}\mathbf{k}\cdot\mathbf{r}_1} |\mathbf{r}_1\rangle \tag{A.4}$$

The Kasteleyn matrix satisfies antiperiodic boundary conditions in the x direction, and since $L_y \to \infty$, we can also assume antiperiodic boundary conditions in the y direction. The appropriate wavevectors are the $\mathbf{k} = k_x\mathbf{u_x} + k_y\mathbf{u_y}$ with

$$k_x \in K_x = \left\{ \frac{(2j+1)\pi}{L_x} \middle| \; j = 0, \ldots, L_x/2 - 1 \right\} \tag{A.5}$$

$$k_y \in K_y = \left\{ \frac{(2j+1)\pi}{L_y} \middle| \; j = 0, \ldots, L_y - 1 \right\}. \tag{A.6}$$

In the new basis, the Kasteleyn matrix takes the following simple form:

$$\mathcal{K}_{\alpha\beta}(\mathbf{k}) = \begin{pmatrix} 2\mathrm{i}\sin k_y & 2\mathrm{i}\sin k_x + 2t\cos(k_x + k_y) \\ 2\mathrm{i}\sin k_x - 2t\cos(k_x + k_y) & -2\mathrm{i}\sin k_y \end{pmatrix}, \tag{A.7}$$

and can easily be inverted:

$$\mathcal{K}^{-1}_{\alpha\beta}(\mathbf{k}) = \frac{1}{\det\left[\mathcal{K}_{\alpha\beta}(\mathbf{k})\right]} \begin{pmatrix} -2\mathrm{i}\sin k_y & -2\mathrm{i}\sin k_x - 2t\cos(k_x + k_y) \\ -2\mathrm{i}\sin k_x + 2t\cos(k_x + k_y) & 2\mathrm{i}\sin k_y \end{pmatrix} \tag{A.8}$$

with

$$\det\left[K_{\alpha\beta}(\mathbf{k})\right] = 4\sin^2 k_x + 4\sin^2 k_y + 4t^2\cos^2(k_x + k_y). \tag{A.9}$$

For two sites $\mathbf{r} = x\mathbf{u_x} + y\mathbf{u_y}$ and $\mathbf{r}' = x'\mathbf{u_x} + y'\mathbf{u_y}$ respectively in sublattices α and β, the Green function element is

$$\mathcal{K}^{-1}_{\mathbf{r},\mathbf{r}'} = \frac{1}{\pi L_x} \sum_{k_x} \mathrm{e}^{-\mathrm{i}k_x(x'-x)} \int_0^{2\pi} \mathrm{d}k_y \, \mathcal{K}^{-1}_{\alpha\beta}(\mathbf{k}) \mathrm{e}^{-\mathrm{i}k_y(y'-y)}. \tag{A.10}$$

In this equation, the integral on $\mathrm{d}k_y$ can, in principle, be done explicitly for any $y' - y$, as will be shown in appendix A.2. To compute the entanglement entropy in the cylinder geometry $|y' - y|$ does not, however, need to be greater than 2, whereas it can attain 3 in the strip geometry.

J. Stat. Mech. (2012) P02003

A.2. Green function elements

The computation of Green functions element requires the evaluation of integrals of the form

$$C_p(k_x) = \int_0^{2\pi} \frac{\cos(p\,k_y)}{4\sin^2 k_x + 4\sin^2 k_y + 4t^2\cos^2(k_x+k_y)}\,\mathrm{d}k_y \tag{A.11}$$

$$S_p(k_x) = \int_0^{2\pi} \frac{\sin(p\,k_y)}{4\sin^2 k_x + 4\sin^2 k_y + 4t^2\cos^2(k_x+k_y)}\,\mathrm{d}k_y, \tag{A.12}$$

with p an even integer (otherwise the integrals are simply zero by symmetry). Both integrands are π-periodic and, following Bioche's rules, we can make the change in variables $u = \tan k_y$. We get

$$C_p(k_x) = \frac{1}{2}\int_{-\infty}^{+\infty} \frac{T_p[(1+u^2)^{-1/2}]\,\mathrm{d}u}{u^2[1+(1+t^2)\sin^2 k_x] - ut^2\sin(2k_x) + \sin^2 k_x + t^2\cos^2 k_x} \tag{A.13}$$

$$S_p(k_x) = \frac{1}{2}\int_{-\infty}^{+\infty} \frac{u(1+u^2)^{-1/2}\,U_{p-1}\left[(1+u^2)^{-1/2}\right]\,\mathrm{d}u}{u^2[1+(1+t^2)\sin^2 k_x] - ut^2\sin(2k_x) + \sin^2 k_x + t^2\cos^2 k_x} \tag{A.14}$$

where $T_p(x)$ and $U_{p-1}(x)$ are the Chebyshev polynomials of the first and second kind, respectively:

$$T_p(\cos\theta) \;\; = \cos p\theta \tag{A.15}$$

$$U_{p-1}(\cos\theta) = \frac{\sin p\theta}{\sin\theta}. \tag{A.16}$$

For p even $T_p(-x) = T_p(x)$ and $U_{p-1}(-x) = -U_{p-1}(x)$. Therefore, both integrands in equations (A.13) and (A.14) are *rational* functions of u, as it should be. C_p and S_p can then be calculated by residue. Closing the contour by a large circle in the upper-half plane, two poles will contribute to the integral. The first pole is at

$$u = \frac{t^2\sin k_x\cos k_x + \mathrm{i}\sqrt{t^2+\sin^2 k_x+\sin^4 k_x}}{1+(1+t^2)\sin^2 k_x} \tag{A.17}$$

and is of order 1. The second one at $u = i$ is there if $p \neq 0$ and is of order $p/2$. Although the residue calculation for any even p is, in principle, straightforward, the procedure becomes more and more cumbersome when p gets larger. Only for $p = 0$ do we get a simple (known [16]) result:

$$C_0(k_x) = \frac{\pi/2}{\sqrt{t^2+\sin^2 k_x+\sin^4 k_x}}. \tag{A.18}$$

From these we can get access to all the Green function elements. The simplest are along the same horizontal line and only require the knowledge of C_0:

$$\mathcal{K}^{-1}_{2\ell\mathbf{u}_x} = 0 \tag{A.19}$$

$$\mathcal{K}^{-1}_{(2\ell+1)\mathbf{u}_x} = \frac{1}{L_x}\sum_{k_x} \frac{\sin k_x\sin(2\ell+1)k_x}{\sqrt{t^2+\sin^2 k_x+\sin^4 k_x}}. \tag{A.20}$$

J. Stat. Mech. (2012) P02003

For the cylinder geometry, the knowledge of C_0, C_2 and S_2 is sufficient. For the strip geometry, C_4 and S_4 are also needed. To compute the entanglement entropy in the Kitaev–Preskill geometry, it is easier to evaluate the double integral ($L_x \to \infty$) in equation (A.10) numerically.

Appendix B. Closed-form formula for $S_{n=\infty}$ in the cylinder geometry

As explained in the text, the maximum probability corresponds to a simple configuration with all boundary spins up. Then, a natural way to proceed would be to use equation (27) and try to evaluate the resulting determinant. This method is most certainly viable, but we will follow another path. In the dimer language, the probability we are looking for is given by

$$p_{\max} = \lim_{L_y \to \infty} \frac{[Z_{\mathrm{cyl}}(L_x, L_y/2)]^2}{Z_{\mathrm{cyl}}(L_x, L_y)}, \tag{B.1}$$

where $Z_{\mathrm{cyl}}(L_x, h)$ counts the number of dimer coverings on a finite cylinder of circumference L_x and height h. Despite the loss of translational invariance in the y direction, Z_{cyl} can still be evaluated in closed form, as is shown in section B.1. From this $p_{\max}$ can easily be calculated, see appendix B.2.

B.1. Dimer coverings on a finite cylinder

Let Z_{cyl} be the partition we are looking for. Using (skew) translational invariance along the x axis, one gets (recall $K_x = \{(2m-1)\pi/L_x, 1 \le m \le L_x/2\}$):

$$Z_{\mathrm{cyl}}(L_x, L_y)^2 = \prod_{k_x \in K_x} \det \left[\mathcal{K}^{(x)}_{1 \le i,j \le 2L_y} \right]. \tag{B.2}$$

In other words, the Kasteleyn matrix is block-diagonal with $L_x/2$ blocks of size $2L_y$. Setting $t_x = t\mathrm{e}^{\mathrm{i}x}$ and $s_x = 2\mathrm{i}\sin x$

$$\mathcal{K}^{(x)} = \begin{pmatrix}
0 & s_x & 1 & t_x & 0 & & & & & & & \\
s_x & 0 & -t_x & -1 & 0 & & & & & & & \\
-1 & \bar{t}_x & 0 & s_x & 1 & t_x & & & & & & \\
-\bar{t}_x & 1 & s_x & 0 & -t_x & -1 & & & & & & \\
0 & 0 & -1 & \bar{t}_x & 0 & s_x & 1 & t_x & & & & \\
0 & 0 & -\bar{t}_x & 1 & s_x & 0 & -t_x & -1 & & & & \\
 & & & & & & -1 & \bar{t}_x & 0 & s_x & 1 & t_x \\
 & & & & & & -\bar{t}_x & 1 & s_x & 0 & -t_x & -1 \\
 & & & & & & & & -1 & \bar{t}_x & 0 & s_x \\
 & & & & & & & & -\bar{t}_x & 1 & s_x & 0
\end{pmatrix}. \tag{B.3}$$

Although it is not easy to diagonalize $\mathcal{K}^{(x)}$, its determinant can be exactly evaluated using

J. Stat. Mech. (2012) P02003

the perturbation trick. To do so, we introduce

$$\mathcal{K}_0^{(x)} = \begin{pmatrix}
0 & s_x & 1 & t_x & 0 & & & & & & -1 & -\bar{t}_x \\
s_x & 0 & -t_x & -1 & 0 & & & & & & \bar{t}_x & 1 \\
-1 & \bar{t}_x & 0 & s_x & 1 & t_x & & & & & & \\
-\bar{t}_x & 1 & s_x & 0 & -t_x & -1 & & & & & & \\
0 & 0 & -1 & \bar{t}_x & 0 & s_x & 1 & t_x & & & & \\
0 & 0 & -\bar{t}_x & 1 & s_x & 0 & -t_x & -1 & & & & \\
 & & & & & & -1 & \bar{t}_x & 0 & s_x & 1 & t_x \\
 & & & & & & -\bar{t}_x & 1 & s_x & 0 & -t_x & -1 \\
-1 & -t_x & & & & & & & -1 & \bar{t}_x & 0 & s_x \\
t_x & 1 & & & & & & & -\bar{t}_x & 1 & s_x & 0
\end{pmatrix}. \tag{B.4}$$

This amounts to putting antiperiodic boundary condition along the y axis for the total Kasteleyn matrix. $\mathcal{K}_0^{(x)}$ is block skew circulant, and it can be diagonalized in Fourier space. In particular, its determinant can be easily evaluated:

$$\det \mathcal{K}_0^{(x)} = \prod_{k_y \in K_y} \Delta(k_x, k_y) \tag{B.5}$$

$$\Delta(k_x, k_y) = 4\sin^2 k_x + 4\sin^2 k_y + 4t^2 \cos^2(k_x + k_y), \tag{B.6}$$

where $K_y = \{(2m-1)\pi/L_y, 1 \leq m \leq L_y\}$. This allows us to express $\det \mathcal{K}^{(x)}$ as

$$\frac{\det \mathcal{K}^{(x)}}{\det \mathcal{K}_0^{(x)}} = \det\left(1 + \left[\mathcal{K}_0^{(x)}\right]^{-1}\left[\mathcal{K}^{(x)} - \mathcal{K}_0^{(x)}\right]\right) = \det M_4^{(x)} \tag{B.7}$$

$\mathcal{K}^{(x)} - \mathcal{K}_0^{(x)}$ is a matrix with only eight non-zero elements, and using elementary row–column manipulations, the determinant can be reduced to a 4×4:

$$M_4^{(x)} = \begin{pmatrix} z & -a & w & -\mathrm{i}b \\ -a & z & \mathrm{i}b & -w \\ -\bar{w} & \mathrm{i}b & \bar{z} & a \\ -\mathrm{i}b & \bar{w} & a & \bar{z} \end{pmatrix} \qquad (z, w, a, b) \in \mathbb{C} \times \mathbb{C} \times \mathbb{R} \times \mathbb{R}. \tag{B.8}$$

After some algebra, we get the following formulae for the coefficients:

$$z = \frac{1}{2} + \frac{2}{L_y} \sum_{k_y} \frac{\sin^2 k_x + \mathrm{i}\left[\sin(2k_y) - t^2 \sin(2k_x + 2k_y)\right]}{\Delta(k_x, k_y)} \tag{B.9}$$

$$a = \frac{2t}{L_y} \sum_{k_y} \frac{\cos k_x}{\Delta(k_x, k_y)} \tag{B.10}$$

$$w = \frac{2\mathrm{i}t}{L_y} \sum_{k_y} \frac{\sin k_x \, \mathrm{e}^{-\mathrm{i}k_x}}{\Delta(k_x, k_y)} \tag{B.11}$$

$$b = \frac{2}{L_y} \sum_{k_y} \frac{\sin k_x}{\Delta(k_x, k_y)}. \tag{B.12}$$

J. Stat. Mech. (2012) P02003

The number of dimer coverings on the triangular lattice with cylindrical boundary conditions is then given by

$$Z_{\rm cyl}(L_x,L_y)=\prod_{k_x}\left\{\det\left(M_4^{(x)}\right)\times\prod_{k_y}\Delta(k_x,k_y)\right\}^{1/2}. \tag{B.13}$$

Evaluating the determinant, we finally get the following closed formula for the partition function:

$$Z_{\rm cyl}(L_x,L_y)=\prod_{k_x}\left\{A(k_x)\times\prod_{k_y}\left[\Delta(k_x,k_y)\right]^{1/2}\right\}, \tag{B.14}$$

with

$$\begin{aligned}A(k_x)&=\left(t^2+\sin^2 k_x+\sin^4 k_x\right)d(k_x)^2+(\sin^2 k_x-t\cos k_x)d(k_x)+1/4+\varepsilon(k_x)^2\\ d(k_x)&=\frac{2}{L_y}\sum_{k_y}\frac{1}{\Delta(k_x,k_y)}\\ \varepsilon(k_x)&=\frac{2}{L_y}\sum_{k_y}\frac{\sin(2k_y)-t^2\sin(2k_x+2k_y)}{\Delta(k_x,k_y)}.\end{aligned} \tag{B.15}$$

B.2. Exact formula for $S_{n=\infty}$

The maximum probability is in the thermodynamic limit given by

$$p_{\rm max}=\lim_{L_y\to\infty}\frac{\left[Z_{\rm cyl}(L_y/2,L_x)\right]^2}{Z_{\rm cyl}(L_y,L_x)} \tag{B.16}$$

$$=\prod_{k_x}\left(\lim_{L_y\to\infty}A(x)\right). \tag{B.17}$$

Equation (B.17) follows from equation (B.16) using Euler–Maclaurin's formula on the ratio of terms involving $\Delta(k_x,k_y)$, coming from equation (B.13). Using equation (A.18), we also have

$$\lim_{L_y\to\infty}{\rm d}(k_x)=\frac{1}{2\sqrt{t^2+\sin^2 k_x+\sin^4 k_x}}, \tag{B.18}$$

while $\lim_{L_y\to\infty}\varepsilon(k_x)=0$ because the integrand has a symmetry center solution of $\sin(2k_y)=t^2\sin(2k_x+2k_y)$. In the end we obtain

$$S_\infty=-\ln p_{\rm max}=-\sum_{k_x=(2m-1)\pi/L}^{1\le m\le L/2}\ln\left(\frac{1}{2}+\frac{1}{2}\frac{\sin^2 k_x-t\cos k_x}{\sqrt{t^2+\sin^2 k_x+\sin^4 k_x}}\right). \tag{B.19}$$

J. Stat. Mech. (2012) P02003

B.3. Asymptotic expansion

At $t = 0$, the subleading constant in the $L \to \infty$ asymptotic expansion just follows from the Euler–Maclaurin formula. We find

$$s_\infty(t = 0) = 0. \tag{B.20}$$

Some additional care must be taken in the case $t > 0$. The function

$$f(k) = -\ln\left(\frac{1}{2} + \frac{1}{2}\frac{\sin^2 k - t\cos k}{\sqrt{t^2 + \sin^2 k + \sin^4 k}}\right) \tag{B.21}$$

actually diverges as $f(k) \sim -2\ln k$—independent of t—when $k \to 0$. The asymptotics can be obtained by applying the Euler–Maclaurin formula on $\sum_k [f(k) + 2\ln k]$ while applying Stirling's formula on the remaining 'linearized' term $-\sum_k 2\ln k$. Doing so we finally obtain the topological term

$$s_\infty(t > 0) = -\ln 2. \tag{B.22}$$

Only the linearized term actually contributes to the constant. Indeed, it is universal and should not be affected by the short-distance (i.e. high momentum k) details of the model.

References

[1] Holzhey C, Larsen F and Wilczek F, *Geometric and renormalized entropy in conformal field theory*, 1994 *Nucl. Phys.* B **424** 443

[2] Vidal G, Latorre J I, Rico E and Kitaev A, *Entanglement in quantum critical phenomena*, 2003 *Phys. Rev. Lett.* **90** 227902

[3] Korepin V E, *Universality of entropy scaling in one-dimensional gapless models*, 2004 *Phys. Rev. Lett.* **92** 096402

[4] Calabrese P and Cardy J, *Entanglement entropy and quantum field theory*, 2004 *J. Stat. Mech.* P06002

[5] Hamma A, Ionicioiu R and Zanardi P, *Ground state entanglement and geometric entropy in the Kitaev model*, 2005 *Phys. Lett.* A **337** 22

[6] Kitaev A and Preskill J, *Topological entanglement entropy*, 2006 *Phys. Rev. Lett.* **96** 110404

[7] Levin M and Wen X-G, *Detecting topological order in a ground state wavefunction*, 2006 *Phys. Rev. Lett.* **96** 110405

[8] Haque M, Zozulya O and Schoutens K, *Entanglement entropy in fermionic laughlin states*, 2007 *Phys. Rev. Lett.* **98** 060401
Zozulya O, Haque M, Schoutens K and Rezayi E H, *Bipartite entanglement entropy in fractional quantum Hall states*, 2007 *Phys. Rev.* B **76** 125310

[9] Friedman B A and Levine G C, *Topological entropy of realistic quantum Hall wavefunctions*, 2008 *Phys. Rev.* B **78** 035320

[10] Läuchli A M, Bergholtz E J, Suorsa J and Haque M, *Disentangling entanglement spectra of fractional quantum Hall states on torus geometries*, 2010 *Phys. Rev. Lett.* **104** 156404

[11] Furukawa S and Misguich G, *Topological entanglement entropy in the quantum dimer model on the triangular lattice*, 2007 *Phys. Rev.* B **75** 214407

[12] Moessner R and Sondhi S, *Resonating valence bond phase in the triangular lattice quantum dimer model*, 2001 *Phys. Rev. Lett.* **86** 1881

[13] Kitaev A Y, *Fault-tolerant quantum computation by anyons*, 2003 *Ann. Phys., NY* **303** 2

[14] Misguich G, Serban D and Pasquier V, *Quantum dimer model on the Kagome lattice: solvable dimer-liquid and Ising Gauge theory*, 2002 *Phys. Rev. Lett.* **89** 137202

[15] Rokhsar D S and Kivelson S A, *Superconductivity and the quantum hard-core dimer gas*, 1988 *Phys. Rev. Lett.* **61** 2376

[16] Fendley P, Moessner R and Sondhi S L, *Classical dimers on the triangular lattice*, 2002 *Phys. Rev.* B **66** 214513

[17] Ioselevich A, Ivanov D A and Feigelman M V, *Ground-state properties of the Rokhsar–Kivelson dimer model on the triangular lattice*, 2002 *Phys. Rev.* B **66** 174405

J. Stat. Mech. (2012) P02003

[18] Stéphan J-M, Furukawa S, Misguich G and Pasquier V, *Shannon and entanglement entropies of one- and two-dimensional critical wavefunctions*, 2009 *Phys. Rev.* B **80** 184421
[19] Kasteleyn P W, *The statistics of dimers on a lattice, Part I*, 1961 *Physica* **27** 1209
[20] Fisher M E and Stephenson J, *Statistical mechanics of dimers on a plane lattice. II. Dimer correlations and Monomers*, 1963 *Phys. Rev.* **132** 1411
[21] Flammia S T, Hamma A, Hughes T L and Wen X-G, *Topological entanglement Rényi entropy and reduced density matrix structure*, 2009 *Phys. Rev. Lett.* **103** 261601
[22] Vishwanath A, Balents L and Senthil T, *Quantum criticality and deconfinement in phase transitions between valence bond solids*, 2004 *Phys. Rev.* B **69** 224416
[23] Ardonne E, Fendley P and Fradkin E, *Topological order and conformal quantum critical points*, 2004 *Ann. Phys., NY* **310** 493
[24] Papanikolaou S, Luijten E and Fradkin E, *Quantum criticality, lines of fixed points, and phase separation in doped two-dimensional quantum dimer models*, 2007 *Phys. Rev.* B **76** 134514
[25] Fradkin E and Moore J E, *Entanglement entropy of 2D conformal quantum critical points: hearing the shape of a quantum drum*, 2006 *Phys. Rev. Lett.* **97** 050404
[26] Hsu B, Mulligan M, Fradkin E and Kim E-A, *Universal entanglement entropy in two-dimensional conformal quantum critical points*, 2009 *Phys. Rev.* B **79** 115421
[27] Oshikawa M, *Boundary conformal field theory and entanglement entropy in two-dimensional quantum Lifshitz critical point*, 2010 arXiv:1007.3739
[28] Hsu B and Fradkin E, *Universal behavior of entanglement in 2D quantum critical dimer models*, 2010 *J. Stat. Mech.* P09004
[29] Stéphan J-M, Misguich G and Pasquier V, *Rényi entropy of a line in two-dimensional Ising models*, 2010 *Phys. Rev.* B **82** 125455
[30] Zaletel M P, Bardarson J H and Moore J E, *Logarithmic terms in entanglement entropies of 2D quantum critical points and Shannon entropies of spin chains*, 2011 *Phys. Rev. Lett.* **107** 020402
[31] Stéphan J-M, Misguich G and Pasquier V, *Phase transition in the Rényi–Shannon entropy of Luttinger liquids*, 2011 *Phys. Rev.* B **84** 195128
[32] Kasteleyn P W, *Dimer statistics and phase transitions*, 1963 *J. Math. Phys.* **4** 287
[33] Fradkin E, Huse D A, Moessner R, Oganesyan V and Sondhi S L, *On bipartite Rokhsar–Kivelson points and Cantor deconfinement*, 2004 *Phys. Rev.* B **69** 224415
[34] Alet F, Jacobsen J L, Misguich G, Pasquier V, Mila F and Troyer M, *Interacting classical dimers on the square lattice*, 2005 *Phys. Rev. Lett.* **94** 235702
[35] Henley C L, *From classical to quantum dynamics at Rokhsar–Kivelson points*, 2004 *J. Phys.: Condens. Matter* **16** S891
[36] Temperley H N V and Fisher M E, *Dimer problem in statistical mechanics—an exact result*, 1961 *Philos* **6** 68
[37] McCoy B M and Wu T T, 1973 *The Two-Dimensional Ising Model* (Cambridge, MA: Harvard University Press)
[38] Dubail J and Stéphan J-M, *Universal behavior of a bipartite fidelity at quantum criticality*, 2011 *J. Stat. Mech.* L03002
[39] Li Hui and Haldane F D M, *Entanglement spectrum as a generalization of entanglement entropy: identification of topological order in non-Abelian fractional quantum Hall effect states*, 2008 *Phys. Rev. Lett.* **101** 010504
[40] Wen X-G, *Chiral Luttinger liquid and the edge excitations in the fractional quantum Hall states*, 1990 *Phys. Rev.* B **41** 12838
[41] Thomale R, Sterdyniak A, Regnault N and Andrei Bernevig B, *Entanglement gap and a new principle of adiabatic continuity*, 2010 *Phys. Rev. Lett.* **104** 180502
[42] Cardy J L and Peschel I, *Finite-size dependence of the free energy in two-dimensional critical systems*, 1988 *Nucl. Phys.* B **300** 377
[43] Isakov S V, Hastings M B and Melko R G, *Topological entanglement entropy of a Bose–Hubbard spin liquid*, 2011 *Nature Phys.* **7** 772
[44] Zhang Y, Grover T and Vishwanath A, *Topological entanglement entropy of Z2 spin liquids and lattice Laughlin states*, 2011 *Phys. Rev.* B **84** 075128
[45] Levin M and Wen X G, *String–net condensation: a physical mechanism for topological phase*, 2005 *Phys. Rev.* B **71** 045110

J. Stat. Mech. (2012) P02003